Digest Journal of Nanomaterials and Biostructures Vol. 9, No. 2, April - June 2014, p. 627 - 639

CORROSION INHIBITION OF NANOCOMPOSITE BASED ON ACRYLAMIDE COPOLYMERS /MAGNETITE FOR STEEL

A. M. ATTA[a,b*], G. A. EL-MAHDY[a, c], H. A. AL-LOHEDAN[a],
S. A. Al HUSSAIN[a, d],
[a]*Surfactants research chair, King Saud University, Chemistry Department, College of Science, P.O.Box - 2455, Riyadh - 11451, Saudi Arabia*
[b]*Petroleum application department, Egyptian petroleum research institute, Cairo, Egypt.*
[c]*Chemistry department, Helwan university, Helwan, Cairo, Egypt.*
[d]*Chemistry department, faculty of science, Al- Imam Muhammad Ibn Saud Islamic University.*

The methods for the design of highly corrosion resistance nanocomposite on the surface of steel with oxide layers have been described. Self-stabilized magnetic polymeric nanoparticles of coated sodium 2-acrylamido-2-methyl propane sulfonate-co- N-Isopropyl Acrylamide/magnetite, NIPAAm/AMPS-Na/Fe_3O_4 , was prepared by surfactant-free radical polymerization using N, N-methylenebisacrylamide (MBA) as crosslinker, and potassium persulfate (KPS) as an initiator in the presence of hydrophilic poly(vinyl pyrrolidone) coated magnetite particles. The chemical structures of the modified NIPAAm/AMPS-Na/Fe_3O_4 were confirmed by FTIR analysis. The morphology and the particle size distributions of the NIPAAm/AMPS-Na/Fe_3O_4 composite were observed and analyzed by transmission electron microscopy (TEM). The average Fe_3O_4 content of NIPAAm/AMPS-Na/Fe_3O_4 was determined by thermogravimetric analysis (TGA). The inhibitive action of NIPAAm/AMPS-Na/magnetite nanogel on corrosion of steel in 1 M HCl solution was investigated through polarization and electrochemical impedance spectroscopy (EIS). The increase in inhibition efficiency with inhibitor concentration is associated with a shift of both cathodic and anodic branches of the polarization curves towards lower current densities and suggested that NIPAAm/AMPS-Na/magnetite nanogel acted as mixed type inhibitor. The results indicate good agreement between the values of inhibition efficiency (IE%) as obtained from the impedance technique and polarization measurements.

(Received February 1, 2014; Accepted May 30, 2014)

Keyword: Magnetite, Nanoparticle, nanocomposite, sodium 2-acrylamido-2-methyl propane sulfonate-co-N-isopropyl acrylamide, Nanogels, corrosion inhibitor

1. Introduction

A new generation of anticorrosion materials that both possesses passive matrix functionality and actively responds to changes in the local environment has prompted great interest from material scientists. The nanometer scaled materials have gained much attention due primarily to the novel properties induced by their high surface-to-volume ratio [1]. Iron oxide nanoparticles and composites attracted great attention to use as protective coatings and anticorrosive materials [2-5]. The roles of the magnetite particles in the polymer matrix composite are to obtain active protection to corrosive processes, to increase the barrier properties for a longer time and to decrease the penetration of aggressive species that promote corrosion when the coated metal is exposed to a corrosive environment [5]. Recently, the smart materials were designed to be sensitive to various external and internal stimuli, thereby enhancing the surface functionality of materials [6]. The coats response action depends on the functionalities that the coatings attain

*Corresponding author: aatta@ksu.edu.sa

during their preparation. The production and applications of the highly dispersed polymer coated magnetite nanoparticles as corrosion inhibitors were previously discussed [7-8]. In this respect, the using of nanogel particles in the field of corrosion inhibition protection for steel instead of normal organic inhibitors produced uniform thin film (without any pine hole due to crosslinked polymers) on the surface of steel to cover all surface without any defects which provide advantages over normal organic inhibitors [7]. The active corrosion protection of these materials aims to restore material properties (functionality) when the passive coating matrix is broken and corrosion of substrate has started. The composite has to release the active material within a short time and acts as a local trigger for the mechanism that heals the defect.

Magnetite–polymeric nanoparticles (M-P NPs), made from organic and inorganic components, have unique characteristics due to the specific properties of the blend. The constituents of an M-P NP play different roles: the polymeric matrix acts as a shell, reservoir, and vehicle for the active component, whereas magnetite is the active component which has ability to form anticorrosive layers for steel in atmospheric and corrosive solutions. In this respect, several approaches have been reported in the literature for synthesis of magnetite-polymer nanoparticles. The technique used to form a magnetite core with a polymer shell nanoparticle is polymerization which is a known bottom-up technique [9-13]. Another interesting technique to prepare magnetite–polymeric nanoparticles, not popularly used as much, is the top-down techniques which based on emulsion techniques to form polymeric nanoparticles including emulsion evaporation, emulsion diffusion, salting out, and nano-precipitation [14-17]. It is based on hydrophobic–hydrophilic interactions, as well as ionic and Van der Walls forces, for nanoparticles formation. We sought to extend bottom-up technique to the preparation of core-shell nanoparticles with well-defined shells composed of crosslinked poly (sodium 2-acrylamido-2-methyl propane sulfonate – co-N-isopropyl acrylamide), AMPS-Na/NIPAAm, nanogels. It was expected that the crosslinked AMPS-Na/NIPAAm magnetite nanogels have ability to form thin films through interaction between the metal surface and the inhibitor molecules and consequently increases the covered surface by the inhibitor. That consequently decreases the attack of the metal surface by the aggressive medium. Moreover, the chemical structures of AMPS-Na/NIPAAm increase their chemisorption on the surface of steel due to coordinate covalent bond formation between electron pairs of N, O and S atoms in AMPS and NIPAAm with metal surface. On the other hand, it was expected that these copolymers can act as smart thin film coats on the steel surfaces due to NIPAAm polymers have strong sensitivity to various external and internal stimuli (pH and temperature). However, it was expected the presence of such smart materials after exposure to certain impact(s), the active part of the smart coatings responds in order to restore the coating functionality, thus reducing the negative effect of the impact on the coating (self-healing concept) or launching additional properties of the coating interface (bioactivity, detection) [6]. In this respect, the poly(vinyl pyrrolidone), PVP, used as dispersant for magnetite will determine the nature and thickness of the polymer shell, which could in turn affect nanocomposite properties such as particle size and morphology, solubility, and melting behavior. In addition, the polymer shell may protect the core or allow the formation of close-packed particle arrays with fixed antiparticle spacing. The syntheses of core-shell magnetite nanogel hybrid nanoparticles where each iron based core bears a strongly bound polymer coating is described. Their corrosion inhibition for steel in 1M HCl solutions is analyzed.

2. Experimental

2.1 Materials

Anhydrous ferric chloride, potassium iodide and ammonium hydroxide (25%) aqueous solution used as reagent for preparation of magnetite and purchased from Aldrich chemicals Co. Poly(vinyl pyrrolidone) (PVP) with molecular weight 40000 g/mol, potassium peroxodisulfate (KPS) and the accelerator *N*,*N*,*N*_,*N*_-tetramethylethylenediamine (TEMED) were provided by Merck. Sodium 2-acrylamido-2-methylpropane sulfonate (AMPS-Na), *N*,*N*-methylene bisacrylamide (MBA) were purchased from Aldrich Chemical Co. and used without purification. *N*-Isopropylacrylamide was purchased from Tokyo Kasei Kogyo Co., recrystallized in toluene :

hexane (60:40) mixture, and dried under vacuum prior to use. Water was deionized by a Millipore Direct-Q apparatus.

Tests were performed on a rolled steel of the following composition (wt%): 0.14% C, 0.57% Mn, 0.21% P, 0.15% S, 0.37% Si, 0.06% V, 0.03% Ni, 0.03% Cr and the remainder Fe. Steel specimens having a surface area of 0.785 cm^2, were used as working electrode (WE) for polarization and EIS measurements. The exposed area was mechanically abraded with different grades of emery papers and rinsed by distilled water before each electrochemical experiment.

2.2. Preparation Technique

Magnetite nanoparticles synthesis:

Hydrophilic magnetite nanoparticles were prepared according to previous modified method [**8**]. Aqueous solution of ferric chloride was prepared by dissolving of 40 g (0.24 mol) of anhydrous $FeCl_3$ in 300 mL of distilled water to prepare an aqueous solution A. Further, 13.2 g (0.08 mol) of potassium iodide is dissolved in 50ml of distilled water to prepare an aqueous solution B. The aqueous solutions A and B are then mixed together at room temperature and stirred and allowed to reach equilibrium for one hour while bubbling with pure N_2 to keep oxygen free throughout the preparation procedure. A precipitate was filtered out, washed with distilled water, dried at vacuum at 30°C and weighed to determine the reaction yield (95% yield). The filtrate is then heated at of 50 ^oC followed by adding , 100 ml water containing PVP (10 g). Ammonia solution (200 ml, 25%) was added dropwise with stirring while bubbling with pure N_2 to keep oxygen free throughout the preparation procedure to hydrolyze iron ions. Mixing is continued until complete precipitation of black magnetite is achieved. The reaction was continued at the reaction temperature with stirring for 4 hrs. The magnetite nanoparticles were dialyzed against water in 12 000-14 000 Da tubing (Spectrum, Rancho Dominguez, CA) and filtered with a 1 μm polycarbonate membrane (Nuclepore, Whatman, Florham Park, NJ). The precipitate is then left to settle washed with distilled water and ethanol, dried at vacuum at 30 ^oC (the precipitate should dry without heating) and weighed. The percentage yield of reaction is 95.5 %.

Preparation of NIPAAm/AMPS-Na/magnetite nanogel

The poly(NIPAAm-*co*-AMPS-Na) / magnetite nanogel particles were prepared by a surfactant-free emulsion polymerization method using modified semi batch method [18]. In this respect, NPAAm (13.3 mmol), AMPS-Na (1.3 mmol) and MBA (0.67 mmol) and magnetite/ PVP nanoparticle (10 % of the total weight of monomers) was fully dissolved in 98 ml of deionized water. Afterwards, 1 mol L−1 NaOH was added dropwise until the pH was 9. The reaction mixture was heated to 70 ◦C under nitrogen purge to remove the dissolved oxygen in a 250 ml four-necked flask. After 30 min, APS (0.47 mmol) and 60 µL of TEMED dissolved in 2 ml of deionized water was injected to initiate the reaction. After cooling, stable nanogel dispersion, the resultant polymer-coated magnetic nanoparticles were collected with the aid of an external magnetic field, washed with deionized water several times and finally dispersed in 45mL of deionized water. The nanogel were purified by at least five cycles of ultracentrifugation (Beckman model, 25 min at 12,000g), decantation, and redispersion in deionized water.

2.3. Characterization

Fourier transform infrared (FTIR) spectroscopic analysis of the samples was performed using a Spectrum One FTIR spectrometer (Perkin–Bhaskar–Elmer Co., USA).

The morphology and structure of the prepared magnetic nanoparticles were determined using high-resolution transmission electron microscopy (HR-TEM). HR-TEM images of the nanocomposites were recorded using a JEM-2100 F (JEOL, Japan) at an acceleration voltage of 150 kV. The TEM images were obtained at 25 ◦C with a TEM-100XS instrument.

Particle size measurements were performed using a dynamic light scattering (DLS) instrument (Particle Sizing Systems).

Zeta potentials of magnetite and nanogel suspensions were measured at 25 ◦C using a zeta potential analyser (Particle Sizing Systems PSS.NICOMP 380 ZLS, USA). Particle suspensions were diluted with deionized water or 0.05 mol L−1 NaCl prior to measurements.

Thermogravimetric analysis (TGA, Universal V3.5B TA instruments) was used to determine the average Fe_3O_4 content of representative NIPAAm/AMPS-Na/magnetite nanocomposite sample. The Fe_3O_4 content of was given according to the weight percentage of the residue remaining after thermal analysis from room temperature to 1000 °C under nitrogen atmosphere.

2.4. Electrochemical Measurements:

Electrochemical measurements were carried out in a conventional three electrode cylindrical glass cell. Platinum electrode was used as a counter electrode and a saturated calomel electrode (SCE) as the reference electrode. Polarization and EIS studies were conducted using computer controlled a Solartron 1470E system (potentiostat/galvanostat) with Solartron 1455A as frequency response analyzer. Multistate software was used for evaluating the experimental data. All experiments were performed with a frequency ranging from 10 mHz to 10 kHz and peak-to-peak a.c. amplitude of 10 mV. The impedance data were analyzed and fitted with the simulation ZView 3.3c, equivalent circuit software

3. Results and discussion

Because the surface of metal oxide particles consists of metal-OH groups, a widely applicable surface modification technique is required. Surface modification using polymers has recently been reported. Surface grafting of polymers is one of the most effective methods used to achieve these surface modifications, as the surface properties can be widely changed by a variety of functional monomers. It was previously reported that, there are two types of methods for surface modification using polymers. One is a “grafted-to” system in which polymers are adsorbed onto the substrate surface and nanoparticle surface after polymerization [19]. The other type is a “grafted from” system in which the surface-initiated polymerization is carried out on the substrate surface and nanoparticle surface. There is disadvantage for using the “grafted-from” method which usually produces in poor control of molecular weight and molecular weight distribution [20]. In the present work, our aims directed to modify the surface of magnetite with PVP to increase their water dispersability followed by surface-initiated crosslinked polymerization of monomers above their lower critical solution transition temperature (LCST) to control these molecular weight factors using living radical polymerization techniques [21-24]. A highly pure and magnetic magnetite shall be provided. In this respect, magnetite Fe_3O_4 nanoparticles were prepared according to the chemical equation ; $Fe^{3+} + I^- \rightarrow 2\ Fe^{3+} + Fe^{2+} + 1/2\ I^-$. This reaction is based on cheapest and most environmental friendly procedure is based on the co-precipitation method, which involves the simultaneous precipitation of Fe^{2+} and Fe^{3+} ions after reaction of KI with $FeCl_3$. Surface modification of nanoparticles allows for the dispersion and stability of these nanoparticles in various solvents or polymer matrices while they maintain their physical characteristics. The produced iodine was separated during the reaction to easily modify the hydrophilic surface of magnetite after precipitation in basic aqueous media in the presence of PVP as stabilizer. It was proposed that PVP were adsorbed on the Fe_3O_4 particle through chelation between Fe_3O_4 and the amide groups of pyrrolidone ring as illustrated in the Scheme 1.The stabilization of hydrophilic magnetite particles is based steric stabilzation mechanism, which the amide groups of PVP interact with OH group of the hydrophilic magnetite. The preparation of the nanogel containing dispersed iron-oxide nanoparticles can be obtained by interaction of NIPAAm hydrophobic monomer above its LCST with PVP polymer backbone of PVP/magnetite particles to be nuclei to form crosslinked nanogel polymers as described in previous work [25]. In the present work, we used high NIPAAm monomer content with (90 mol %) and AMPS-Na (10 mol %) to increase the interaction between PVP backbone and isopropyl group of NIPAAm to produce NIPAAm/AMPS-Na/magnetite containing hydrophilic AMPS-Na monomer at their surfaces as illustrated in scheme 1.

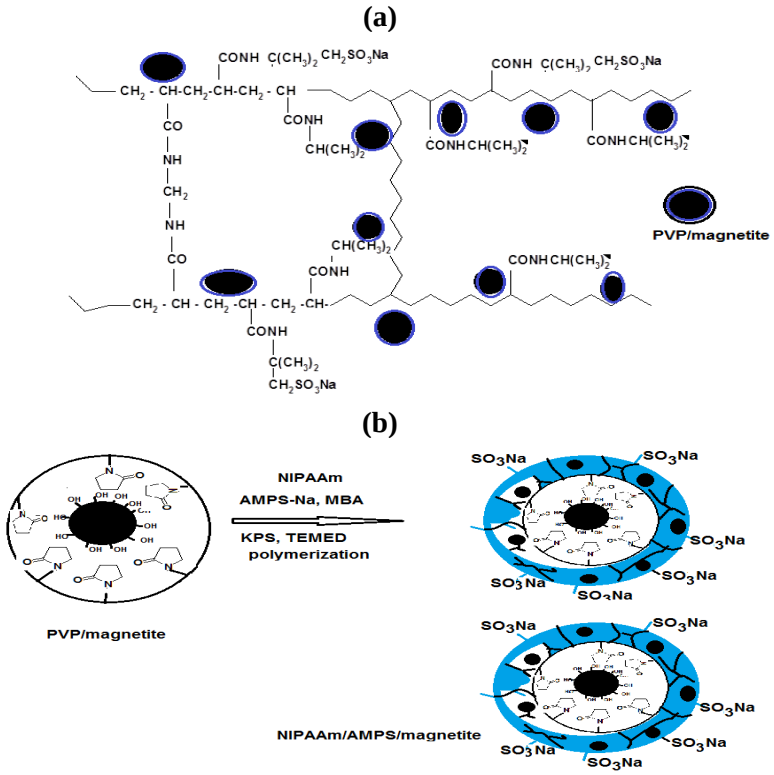

Scheme 2: a) chemical structure and b) schematic presentation of NIPAAm/AMPS-Na/Magnetite.

It was proposed that, as the reaction proceeds, the PNIPAm oligomers form at a temperature above the LCST. At this temperature the degree of crosslinking achieves a certain level, the size of the oligomers exceeds the solubility limit, and PNIPAm coagulates out of the water phase and forms unstable primary particles. These particles undergo growth and coagulation, thereby increasing the surface charge when polymerized with AMPS, until electrostatic stabilization at the surface of PVP magnetite is achieved. When the hydrophilic AMPS monomer is incorporated into the polymerization of NIPAm, the coagulation and nucleation are hastened by the hydrogen-bonding interaction between AMPS and NIPAm molecules. The interaction between PVP/magnetite and NIPAAm/AMPS-Na copolymer might be a factor that decreases the growth of particles throughout the polymerization process.

3.1 Characterization of AA-Na/magnetite composite:

FTIR analysis was used to illustrate the chemical structures of the prepared nano- and micro-particles. In this respect, IR spectra of hydrophilic, and NIPAAm/AMPS-Na/magnetite particles were represented in Figures 1a and b, respectively. It was observed that, the IR spectra of all samples clearly reveal the presence of strong IR absorption bands at between 400 and 700 cm^{-1}, which are the characteristic absorption peaks of Fe-O vibration related to Fe_3O_4. Magnetite formation can be confirmed through the presence of 584 and 637 cm^{-1} bands assigned to stretching and torsional vibration modes of the magnetite. However, in present cases the band for Fe-O shift towards higher wavenumber (570 and 620 cm^{-1}). This may be due to the breaking of the large number of bands for surface atoms, resulting rearrangement of localized electrons on the particle surface and the surface bond force constant increases as Fe_3O_4 is reduced to nanoscale dimension, so that the absorption bands shift to higher wavenumber [26]. To understand the adsorption mechanism of the PVP on the surface of Fe_3O_4 nanoparticles, figure 1a, bands at 3350, 1690, 1430

cm^{-1} attributed to NH stretching, CO amide stretching and C-N stretching, respectively, indicated that PVP adsorbed on the surface of magnetite. Figures 1 b indicated that the characteristic C=O amide band of NIPAAm/AMPS-Na/magnetite (present at 1700 cm^{-1}) is disappeared with the appearance of two new broad bands at 1640 and 1610 cm^{-1} characteristic to asymmetric and symmetric carboxylate stretching. These results revealed that NIPAAm/AMPS-Na was chemisorbed onto the Fe_3O_4 nanoparticles as a carboxylate with both oxygen atoms coordinated symmetrically to Fe atoms. The appearance of band at 3350 cm^{-1} (NH group of MBA, NIPAAm and AMPS) in figure 1 b indicated the crosslinking of NIPAAm and AMPS with MBA crosslinker.

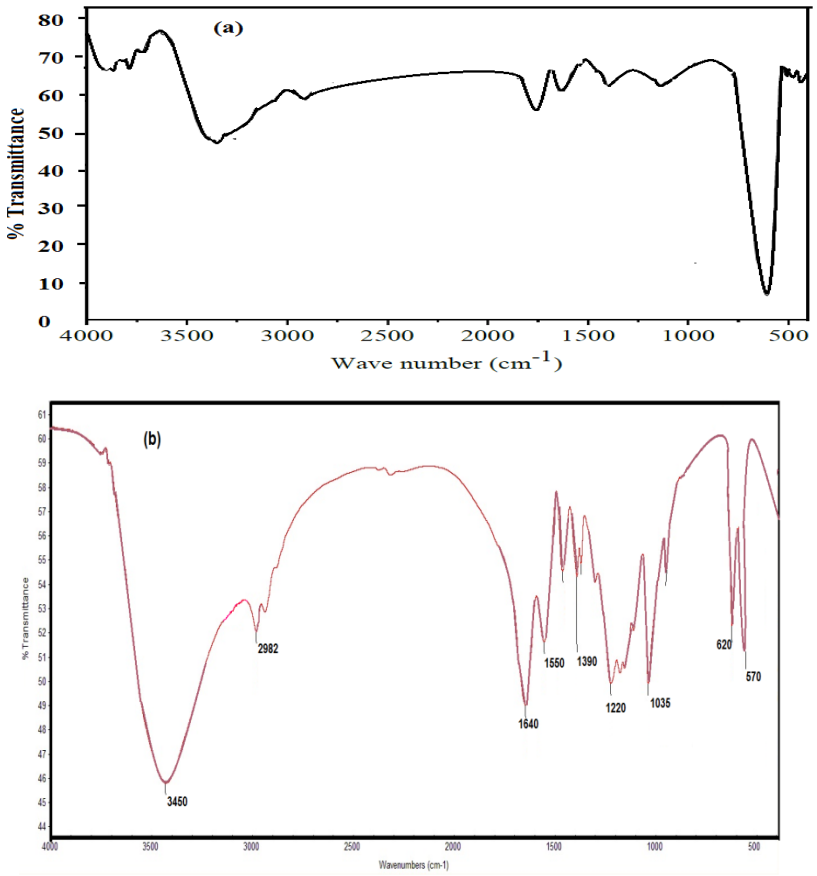

Fig. 1: FTIR spectra of a) PVP/magnetite and b) NIPAAm/AMPS-Na/Magnetite nanogel.

Transmission electron microscopy (TEM) was used to characterize the NIPAAm/AMPS-Na/magnetite nanogel. The NIPAAm/AMPS-Na/magnetite prepared with either hydrophilic magnetite consisted of simple core-shell nanoparticles where the polymer shell is clearly visible (Figure 2). The TEM micrograph showed a good distribution and a small size of the nanoparticles. TEM image of hydrophilic magnetite stabilized with PVP (Figure 2 a) shows defined magnetite nanoparticles with diameter between 5 to 9 nm, but with a strong tendency to form clusters (aggregation). It can be expected that the size of NIPAm/AMPS/magnetite nanogels will be lower than the size of NIPAm/AMPS nanogels prepared without magnetite. It was previously reported that the particle size diameter of NIPAm/AMPS nanogels was ranged from 67-176 nm based on AMPS content (from 2 to 10 mol %) [25]. As expected from scheme 1, the NIPAm/AMPS/magnetite nanogels appear with a smooth, large and completely transparent (fades for a large distance) periphery and the particle size diameter ranged from 20 to 30 nm.

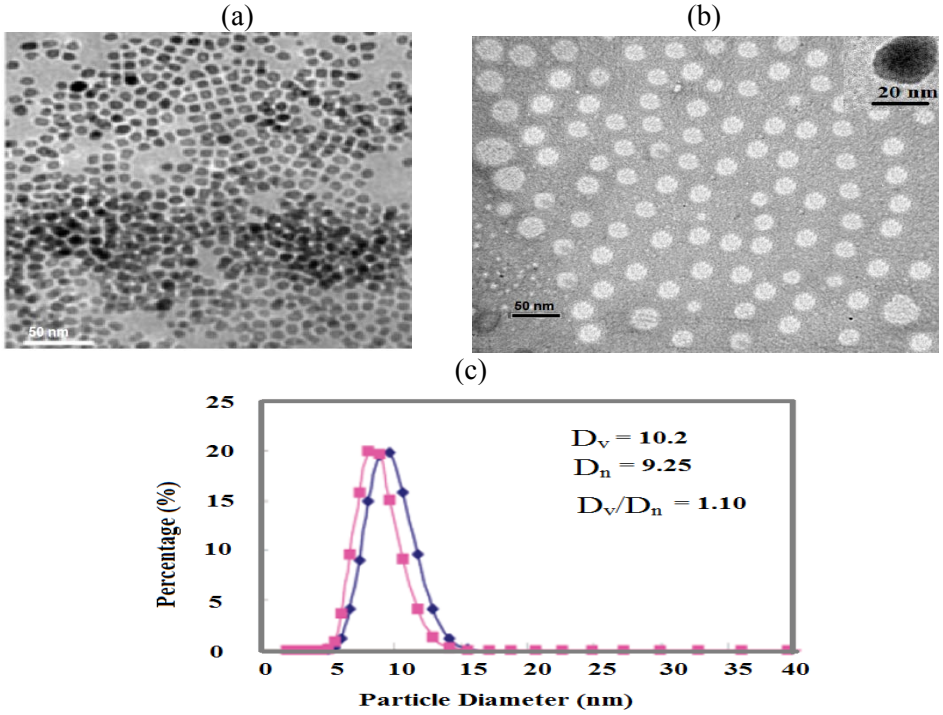

Fig. 2: TEM micrographs of a) PVP/magnetite, b) NIPAAm/AMPS-Na/Magnetite and c) particle size distributions of b) NIPAAm/AMPS-Na/Magnetite nanogel.

The particles spread out completely, because of the hydrated free NIPAm/AMPS chains and the surface is completely transparent. It seems that the NIPAm/AMPS particles show an obvious core–shell structure with a black core and surrounding shadows (figure 2b at high resolution), indicating that the magnetite encapsulated with NIPAm/AMPS nanogels. Moreover, it is noticed that NIPAm/AMPS/ magnetite nanogel dried powder is easy to re-disperse in distilled water to form nanogel solutions. Particle size distribution measurement of NIPAm/AMPS magnetite nanogels indicated that they had a number average diameter (D_n) and volume average diameter (D_v) of 10.2 nm. The polydispersity index (D_v/ D_n) of the particles was 1.1, indicating a very narrow size distribution in aqueous solution (Figure 2c).

DLS measurements of Fe_3O_4 stabilized with PVP and NIPAm/AMPS were represented in Figure 3. The hydrodynamic average particle sizes of Fe_3O_4 stabilized with PVP and NIPAm/AMPS are 12.7 and 26.2 nm, respectively (Fig. 3).

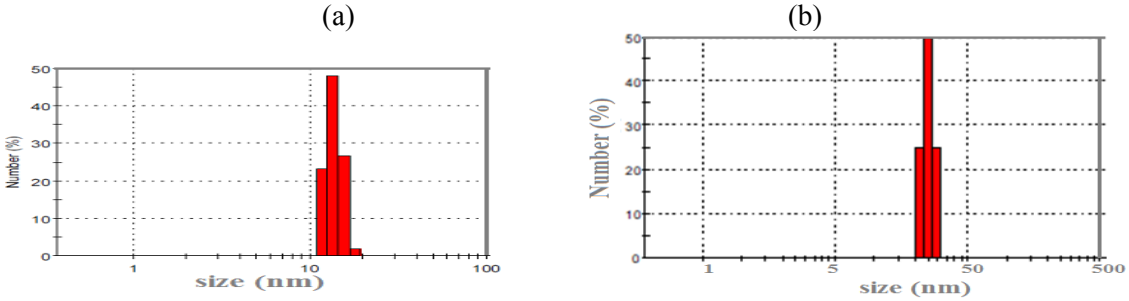

Figure 3: DLS measurements of a) PVP/magnetite and b) NIPAAm/AMPS-Na/Magnetite nanogel.

The data of Fig. 3 indicate that the average particle sizes of Fe_3O_4 stabilized with PVP using this technique are much larger than those obtained using TEM. This is because even in the absence of any external magnetic field, the magnetostatic (magnetic dipole–dipole) interactions

between the particles can cause their agglomeration. The agglomerated ring and loop structures are not seen in TEM imaging, possibly because they are disturbed due to the drying forces present during TEM sample preparation The particle size distribution of core Fe_3O_4 stabilized with crosslinked NIPAm/AMPS shell using DLS are same to that determined by TEM indicated that the formation of core- shell particles reduced the magnetite agglomeration and, consequently, the data of particle size determined by TEM are same to that determined by DLS measurements.

The dispensability and stability of the prepared magnetite NIPAm/AMPS nanogels were estimated using zeta potential measurements. The data of zeta potentials of Fe_3O_4 and Fe_3O_4. NIPAm/AMPS were represented in Figure 4**.** The zeta potentials of Fe_3O_4 and Fe_3O_4. NIPAm/AMPS are −5.93 and −76.73 mV, respectively. It is well known that nanogel particles with higher charge and smaller size distribution are less likely to combine with each other. Zeta potential measurements indicate the successful coating of magnetite nanoparticles. The increase in the negative charge density of the nanogel is attributed to the presence of the sulfonate acid group of AMPS -Na. The highly negative charge on the surface of the nanoparticles reflects the high stability of the nanogel against aggregation because of the repulsion forces between adjacent molecules.

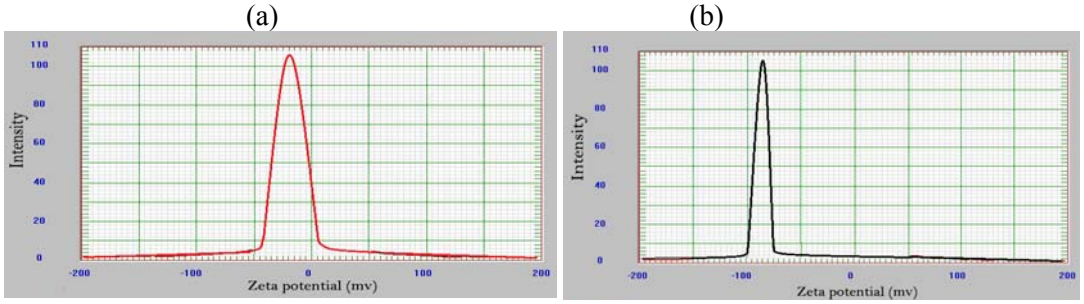

Fig. 4: Zeta potential of a) PVP/magnetite, b) NIPAAm/AMPS-Na/Magnetite and c) particle size distributions of b) NIPAAm/AMPS-Na/Magnetite nanogel in aqueous solution at pH=7.

It is well established that the TGA is an effective tool of analysis to determine the inorganic contents in the polymer composites. The polymer should be decomposed completely when the temperature is high enough, but if there are inorganic materials in the sample, they should remain. TGA of NIPAm/AMPS/ magnetite was represented in Figure 5.

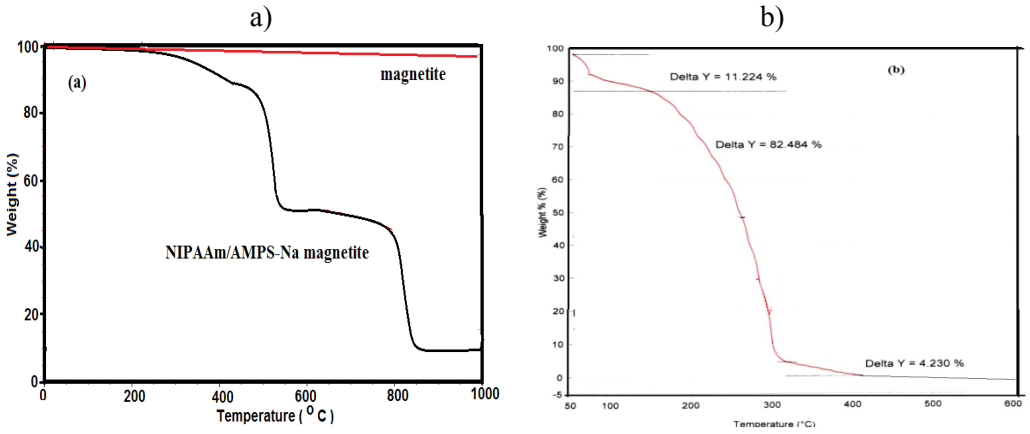

Fig. 5: TGA thermograms of a) magnetite and NIPAAm/AMPS-Na/Magnetite nanogel and b) NIPAAm/AMPS-Na without magnetite.

The organic materials and magnetite of the samples were completely burned to generate gas products and converted into Fe_2O_3 at elevated temperatures, respectively. The magnetite amounts of samples can be estimated from the residual mass percentages. The absolute weight loss

of the uncoated Fe_3O_4 is 3.2% (Figure 5a) for the whole temperature range because of the removal of adsorbed physical and chemical water. Figure 6a shows that the weight loss increased above 200°C, attributed to the loss of PVP layer coated on the MNPs. It is estimated that the weight loss of PVP coated on the Fe_3O_4 nanoparticles is about 3.8%. The NIPAm/AMPS magnetite nanocomposites (Figure 5 a) display two main decomposition stages, and the increment of decomposition temperature can be referred to the catalytic activities of Fe3O4 nanoparticles. The weight loss in the range 220 – 320 °C corresponds to the beginning temperature of the transformation from magnetite to hematite. This transformation appears a multi-step process, which is composed of gradual transformation of the magnetite nanoparticles to maghemite (γ-Fe2O3). The weight loss (5.4%) in the range 297.2 - 318.9 °C is attributed to the transformation from maghemite to hematite (α-Fe2O3). These two thermal events are consistent with the previously reported phase-transformation temperature range of magnetite. This is followed by weight loss within the temperature of 300-470 °C, which is attributed to the thermal decomposition of the crosslinker. Additionally, the second decomposition stage at the temperature range 450-650 °C represents the degradation of polymer backbone and conversion of the remaining material to carbon residues. The sharp weight loss of composite at 688.6 °C is suggested to be due to the thermal decomposition of the polyacrylamide chains backbone. As can be seen in Figure 5, when temperature reached about 850 ^oC the weight of the sample was constant and the residue was 10 %. In addition, there was no increase in weight resulting from the oxidation of Fe_3O_4 to Fe_2O_3, because TGA was carried out under nitrogen atmosphere. This fact indicated that the Fe_3O_4 content for the NIPAm/AMPS/ magnetite was 10%. As shown in Figure 5b, for crosslinked of NIPAm/AMPS without magnetite the first weight loss stage (below 140°C) can be ascribed to the evaporation of water molecules in the polymer matrix, while the other stage beginning at about 200°C was due to the decomposition of amide groups of NIPAm/AMPS.

3.2. Electrochemical impedance spectroscopy (EIS)

The previous section indicated that magnetite nanoparticles core were encapsulated in NIPAm/AMPS shell which contains temperature and pH sensitive NIPAAm and AMPS-Na moieties, respectively. Accordingly. it was expected that, NIPAm/AMPS magnetite nanogels will form thin layer of a smart and active coating on the steel substrates. The high versatility of encapsulation technologies, active agents, and shell components allows selection of the appropriate library of nanocontainers with the desired characteristics (size, sensitivity of the shell, compatibility to the matrix), thereby isolating the problems associated with each individual function **[6].** In this respect, **t**he smart coating concept has provided effective anticorrosion self-healing coatings and bioactive coatings. This work aims to coat the magnetite with the outer surface with pH-sensitive weak polyelectrolytes or other polymers to provide controlled release of the encapsulated magnetite inhibitor. The main advantage of the composite inorganic nanocontainers is their small size (typically <100 nm), making them have ability to form thin coatings. The triggering mechanism of inhibitor release is local changes of the pH value caused by the corrosion process, which in turn cause the pH-sensitive polymer or polyelectrolyte shell to open the pores and release encapsulated inhibitor [6]. In the present work, the prepared NIPAm/AMPS/ magnetite composite was tested as corrosion inhibitors for steel in strong corrosive HCl aqueous solution (1M).

The Nyquist plots for steel in 1 M HCl solution in the presence of different concentrations of NIPAAm/AMPS-Na/magnetite nanogel are shown in Figure 6. The polarization data for the blank solution is depicted in the inset of Figure 6. The Nyquist plots are analyzed in terms of the equivalent circuit composed with classic parallel capacitor (Cdl), polarization resistance (Rp) and solution resistance (Rs) as shown in Figure 7 [27]. It enables the calculation of numerical values corresponding to the physical and/or chemical properties of the electrochemical system under

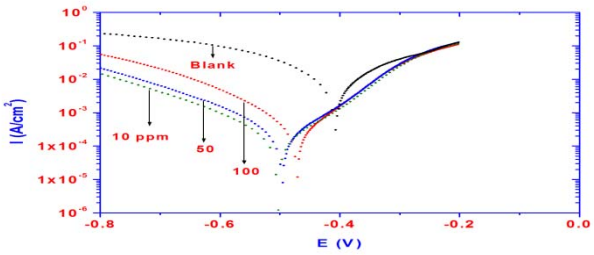

Fig. 6: Polarization curves for steel in 1M HCl solution containing NIPAAm/AMPS-Na/Magnetite having different concentrations.

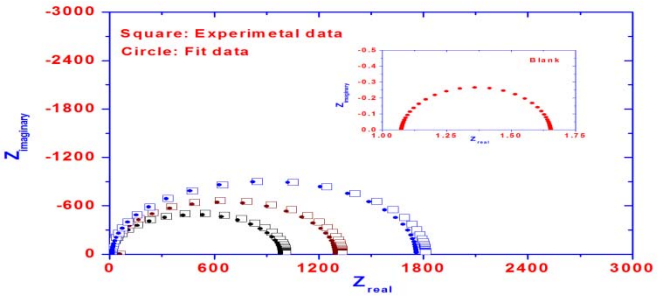

Fig. 7: Nyquist diagram for steel in 1 M HCl solution containing NIPAAm/AMPS-Na/Magnetite having different inhibitor concentrations showing experimental and fit data.

investigation **[28].** Capacitive like clearly distinguishable semicircles were observed at high and low frequencies, which indicate that the corrosion process is mixed control **[29].** The diameter of the semicircle is associated with the polarization resistance and thus the corrosion rate increase with increasing the inhibitor concentration. It can be concluded that the larger the semicircle diameter, the lower is the corrosion rate. The increased diameter of the semicircle in the Nyquist plot for the 250 ppm indicates effective inhibition from the corrosion attack and is reflected by its high polarization resistance. The addition of 100 ppm to the blank solution retains the barrier property to a larger extent compared to that with lower concentrations. The decrease in corrosion rate can be attributed to the formation of a protective film, which hinders the penetration of electrolyte toward the steel substrate. The impedance parameters including polarization resistance Rp, double layer capacitance Cdl are given in Table 1.

Table 1: Inhibition efficiency of PAMPS-Na-co-St / magnetite composite values for steel in 1M HCl with different concentrations of inhibitor calculated by Polarization and EIS methods.

	Polarization Method					EIS Method		
	Ba (mV)	Bc (mV)	E_{corr} (V)	i_{corr} mA/cm^2	IE%	R_p Ohm	Cdl (□F/cm^2)	IE%
Blank	147.00	141.00	-0.4034	7.45	____	1.80	334	____
100 ppm	88.69	101.93	-0.4708	0.284	96.18	1008	91.7	99.80
50	96.46	114.03	-0.4958	0.180	97.57	1331	63.1	99.85
10	104.66	121.34	-0.5022	0.147	98.20	1800	58.1	99.88

It is evident that the polarization resistance Rp increases and double layer capacitance Cdl decreases with the increase of inhibitor concentration. The decrease in Cdl comparing with that in blank solution (without inhibitor), can be attributed to a decrease in local dielectric constant and/ or an increase in the thickness of the electrical double layer. It suggests that the adsorption of inhibitor takes place at the steel/solution interface [30]. The inhibition efficiency (IE%) at different inhibitor concentrations were calculated by using the following equation [31], IE% = 1-

Rp_2 / Rp_1 x 100, where $Rp_1$and Rp_2 are the polarization resistances in presence and absence of the inhibitors, respectively. As shown in Table 1, the polarization resistance and the IE% values increase with an increase in the concentration of inhibitor, while the values of Cdl decrease. The decrease in this capacity with increase in inhibitors concentrations may be attributed to the formation of a protective layer on the electrode surface [32].

3.3. Potentiodynamic polarization measurements

Figure 8 shows the results of the cathodic and anodic polarization curves of steel in 1 M HCl in the absence and presence of different inhibitor concentrations. The cathodic and anodic branches of the polarization curves show lower values of current density compared to the blank solution. The addition of inhibitor to the blank solution is accompanied by a formation of protective layer on the surface. The presence of such films causes a decrease in reaction rate of Fe dissolution and hydrogen reduction on the surface of steel. As a result, both cathodic and anodic branches of the curves are shifted towards lower values of current density. This may be ascribed to adsorption of inhibitor over the corroded surface [33].

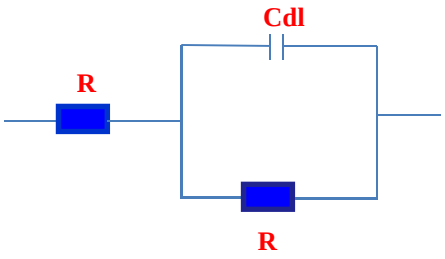

Fig. 8: Equivalent circuit used for fitting the impedance data.

The values of corrosion current densities (Icorr), corrosion potential (Ecorr), the cathodic Tafel slope (Bc), anodic Tafel slope (Ba), as functions of inhibitor concentration, were calculated from the curves of Figure 8 and given in Table 1. Both the anodic and cathodic Tafel slopes change upon addition of inhibitor in 1M HCl solution, which indicates that the inhibitor affects both anodic and cathodic reactions [33] and the inhibitor acts as a mixed-type inhibitor. The presence of inhibitor in the test solution act as adsorptive inhibitor, retarding both cathodic and anodic reaction by blocking the active sites [34-35]. An increase in inhibitor concentration probably increase the number of inhibitor molecules on the steel–solution interface and decrease the corrosion current densities. From the Tafel polarization results it may be concluded that the inhibition mechanism involves blockage of carbon steel surface by the inhibitor molecules via adsorption. The inhibition efficiency (IE%) was calculated using the following equation, IE% = 1- I_2 / I_1, where I_1 and I_2 represent the corrosion current densities in absence and presence of inhibitor, respectively. The calculated values of IE% as functions of inhibitor concentration are given in Table 1. It is evident that the corrosion current decreases substantially and IE% increase with the inhibitor concentration. The corrosion inhibition efficiencies are directly proportional to the amount of adsorbed inhibitor, which controlled the anodic and cathodic reactions during corrosion process. The results suggest that the as-formed protective film gets adsorbed onto the steel substrate, hindering the dissolution of substrate in anodic sites. The suppression of cathodic process can be attributed to the covering of the surface with the adsorbed inhibitor film, indicating that hydrogen reduction was arrested with the protective film. It can be concluded that IE% obtained from EIS and electrochemical polarization curves are in reasonably good agreement.

4. Conclusions

Surfactant-free crosslinking polymerization using an ionic monomer (AMPS-Na) and hydrophobic monomer NIPAAm was used to prepare self-stabilized magnetic polymeric composite particles.

The results showed that the encapsulation of magnetite was successful by using this techniqueThe distribution of magnetite particles inside the NIPAAm/AMPS-Na / magnetite was mainly in the core of the composite magnetic particles.

The NIPAAm/AMPS-Na/magnetite nanogel acts as an excellent corrosion inhibitor as well as a mixed type inhibitor for corrosion of steel in 1M HCl solution.

The inhibition efficiency increases with increase of inhibitor concentration and the inhibition process can be attributed to the adsorption of the inhibitor molecules on the active corrosion sites.

The inhibition efficiency obtained from EIS measurement and electrochemical polarization curves are in reasonably good agreement.

Acknowledgment

This project was supported by King Saud University, The authors extend their appreciation to the Deanship of Scientif Research at King Saud University for funding this work through research group no RGP-VPP-235.

References

[1] H.J. Shin, I.W. Hwang, Y.N. Hwang, Journal of Physical Chemistry B, **107**, 4699 (2003).
[2] C.R. Montoya, H.G. Martins, I.V. de Melo, F. J. Aoki, J.A. Calderón, Electrochimica Acta, http://dx.doi.org/10.1016/j.electacta.07.105 (2013).
[3] Y.I. Kuznetsov, D.B. Vershok, S.F. Timashev, A.B. Solovyeva, P.I. Misurkin, V.A. Timofeeva, S.G. Lakeev, Russ. J. Electrochem. **46**, 1155 (2010).
[4] L.B. Boinovich, S.V. Gnedenkov, D.A. Alpysbaeva, V.S. Egorkin, A.M. Emelyanenko, S.L. Sinebryukhov, A.K. Zaretskaya, Corrosion Science, **55**, 238 (2012).
[5] P. Montoya, F. Jaramillo, J. Calderon, S.I.C. de Torresi, R.M. Torresi, Electrochimica Acta, **55**, 6116 (2010).
[6] D. Shchukin, H. Möhwald, Science 341, p.1458; DOI: 10.1126/science.1242895 (2013).
[7] A.M. Atta, M. Hegazy, O.E. El-Azabawy, H.S. Ismail, Corros.Sci. **53**, 1680 (2011).
[8] G. El Mahdy, A.M. Atta, A. Dyab, H. A. Al-Lohedan, E-Journal of Chemistry, Accepted 11 October 2013.
[9] P. A. Dresco, V.S. Zaitsev, R. J. Gambino, B. Chu, Langmuir, **15**, 1945 (1999).
[10] R. Matsuno, K. Yamamoto, H. Otsuka, A. Takahara, Chem. Mater, **15**, 3 (2003).
[11] S. Lu, J. Ramos, J. Forcada, Langmuir, **23**, 12893 (2007).
[12] A. M. Atta, M. Akel, R. A. Elghazawy, M. Alaa, Polymer Science, Ser. A, **55**, 327 (2013).
[13] G. Mobe, K.Kon-no, K. Kyori, A. Kitahara, J. Coll. Inter. Sci. **93**, 293 (1983).
[14] N. A. D. Burke, H. D. H. Sto¨ver, F. P. Dawson, Chem. Mater., **14**, 4752 (2002).
[15] S.Wizel, S. Margel, A. Gedanken, Polym. Int. **49**, 445 (2000).
[16] K. S. Suslick, M. Fang, T. Hyeon, J. Am.Chem. Soc. **118**, 11960 (1996).
[17] R. Matsuno, K. Yamamoto, H. Otsuka, A. Takahara, Macromolecules **37**, 2203 (2004).
[18] M.A. Akl, A.A. Sarhan, K.R. Shoueir, A. M. Atta, A J Disp Sci Technologies, **34**, 1399 (2013).
[19] H. Ben Ouada, H. Hommel, A. P. Legrand, H. Balard, E.Papirer, J. Colloid Interface Sci., **122**, 441 (1988).
[20] O. Prucker, J. Ru¨ he, Macromolecules, **31**, 592 (1998).

[21] P. P. Quirk, R. T. Mathers, T. Cregger, M. D. Foster, Macromolecules **35**, 9964 (2002).
[22] A. M. Atta, R. A. M. El-Ghazawy, R. K. Farag and S. M. Elsaeed, Polym. Adv. Technol. **22**, 732 (2011).
[23] A. M. Atta , J. Appl. Polym, Sci.**124**, 3276 (2012).
[24] M.A. Akl, A.M. Atta, A. M. Yousef, M. I. Alaa, Polym. Int. **62**, 1667 (2013).
[25] A.M. Atta, Polym. Inter. first published online : 24 MAY 2013, DOI: 10.1002/pi.4537
[26] M. Ma, Y. Zhang, W, Yu, H. Shen, H. Zhang, N. Gu, Colloids and Surfaces A : Physicochem. Eng. Aspects **212**, 219 (2003).
[27] M. Abdel-Gaber, B.A. Abd-El-Nabey, I.M. Sidahmed, A.M. El Zayaday, M. Saadawy, Corrosion Science, **48**, 2765 (2006).
[28] P. Bommersbach, C. Alemany-Dumont, J.P. Millet, B. Normand, Electrochimica Acta, **51**, 4011 (2006).

[29] J.L. Trinstancho-Reye, M. Sanchez-Carrillo, R. Sandoval-Jabalera, V.M. Orozco- Carmon, F. Almeraya-Calderon, J.G. Chacon-Nava, J.G. Gonzalez-Rodriguez, A. Martinez-Villafane, International Journal of Electrochemical Science, **6**, 419 (2011).
[30] M. Lagrenee, B. Mernari, M. Bouanis, M. Traisnel, F. Bentiss, Corros. Sci. **44**, 573 (2002).
[31] H. Ma, S. Chen, L. Niu, S. Zhao, S. Li, D. Li, J. Appl. Electrochem. **32**, 65 (2002).
[32] E. McCafferty, N. Hackerman, J. Electrochem. Soc. **119**, 146 (1972).
[33] G.N. Mu, X.H. Li, Q. Qu, J. Zhou, Corros. Sci., **48**, 445 (2006).
[34] M.A. Amin, K.F. Khaled, Q. Mohsen, H.A.Arida, Corros. Sci., **52**, 1684 (2010).
[35] G. Bereket, A. Yurt, T, Corrosion Science, **43**, 1179 (2001).